APPLIED ORGANOMETALLIC CHEMISTRY
Appl. Organometal. Chem. 2005; **19**: 742–749
Materials, Nanoscience and Catalysis AOC
Published online 22 March 2005 in Wiley InterScience (www.interscience.wiley.com). DOI:10.1002/aoc.872

Macroporous SiC–$MoSi_2$ ceramics from templated hybrid $MoCl_5$–polymethylsilane

Hao Wang[1]*, Xiao-dong Li[1] and Dong-pyo Kim[2]

[1]Key Lab of Ceramic Fiber and Composites, National University of Defense Technology, Changsha 410073, People's Republic of China
[2]Department of Fine Chemical Engineering and Chemistry, Chungnam National University, Taejon 305-764, Korea

Received 8 September 2004; Revised 27 October 2004; Accepted 4 October 2004

A molybdenum-containing preceramic polymer, MoPMS, was synthesized for the first time by HCl elimination of polymethylsilane (PMS) and $MoCl_5$ at room temperature in tetrahydrofuran. The insoluble MoPMS prepared was embedded into the void spaces of a silica colloidal crystal template within the pot life of the polymer and successfully transformed to a three-dimensionally long-range-ordered macroporous SiC–$MoSi_2$ ceramic after pyrolysis at 1400 °C in an argon atmosphere followed by template removal in HF. The bead-inverse macroporous SiC–$MoSi_2$ ceramic, with a ceramic yield of about 88%, exhibits high temperature stability, high BET surface area, and semiconducting behavior. In addition, the macroporous SiC–$MoSi_2$ ceramic was used as a catalyst carrier for platinum–ruthenium coated on the surface of the pores. The preceramic polymer and the ceramic were characterized by IR, thermogravimetric analysis, X-ray diffraction, scanning and transmission electron microscopy, and BET surface area. Copyright © 2005 John Wiley & Sons, Ltd.

KEYWORDS: organometallic polymer; polymethylsilane; porous materials; sacrificial template method; SiC–$MoSi_2$ ceramic

INTRODUCTION

Non-oxide ceramics, such as SiC and Si_3N_4, have attracted considerable interest in recent years, owing to their high strength and high temperature resistance.[1–4] Since the pioneering work of Verbeek and Winter[5] and Yajima *et al*.[6] in the mid 1970s, polymer-based methods used to fabricate these non-oxide ceramics have been paid more attention compared with traditional grinding methods,[7] and many kinds of precursor, such as polycarbosilanes, polysilazanes, polyborazines, and polysilylenemethylenes, have been synthesized and converted to desired shapes, including fibers, films, monoliths and porous structures after pyrolysis.[8–10] The advantages of the polymer-based methods, such as their intrinsic homogeneity on an atomic level and low processing temperatures,[11] stimulate the development of analogous metal-containing preceramic polymers in preparing functional solid-state materials that possess interesting electrical, magnetic and optical properties in addition to desired mechanical characteristics.[12]

Ishikawa *et al*.[13] synthesized an aluminum-containing polymer, polyaluminocarbosilane, and converted it to Si–Al–C–O ceramic fiber that exhibited extraordinary thermal and mechanical stabilities even up to 2200 °C. Manners and coworkers[7,12] synthesized an ion-containing polymer, polyferrocenylsilane, which was then converted to magnetic ceramics with porous or patterned morphologies. Yajima *et al*.[14] prepared titanium-modified polycarbosilane, poly(titanocarbosilane), and converted it to SiC–TiC composites. Kriventsov and coworkers[15,16] synthesized Zr-modified polycarbosilane and converted to SiC/$ZiSi_2$ composites. In addition, many groups have also reported the synthesis of zirconium- or titanium-containing polymers that displayed an enhanced electrical conductivity or unique magnetic behavior.[17,18] However, there have been few reports about molybdenum-containing non-oxide ceramics from polymeric routes, although it is well known that SiC–$MoSi_2$ composites can be used as high-temperature structural materials and heating elements owing to their many novel properties, such as high creep resistance, high oxidation resistance at elevated temperature, high heat conductivity and high electrical conductivity.[19–21]

*Correspondence to: Hao Wang, Key Lab of Ceramic and Fiber Composites, National University of Defense Technology, Changsha 410073, People's Republic of China.
E-mail: whlucky2002@hotmail.com
Contract/grant sponsor: National Research Lab; Contract/grant number: M10400000061-04J0000-06110.
Contract/grant sponsor: Chinese Natural Science Fund; Contract/grant number: 59972042.

It is obvious that the metal-containing polymers have more versatile processibility, compared with the conventional powder processing technologies that are commonly used to produce large particles with simple designs.[7,11] However, an improved approach with higher precision formability is being demanded for newly emerging applications for electrically conductive components or small, precision parts with complex geometries, e.g. microelectrodes, microsensors or micromechanical and electronic devices. As an example, porous materials, such as porous carbon,[22] polymer[23,24] and ceramics,[25–27] have been successfully fabricated from the sacrificial template method. Thus, one may anticipate that electrically resistive ceramic filters or membranes could be prepared by infiltrating with viscous precursors into sacrificial templates, which combine self-cleaning functions with high temperature stability.

In this paper we report on the synthesis of a high molecular weight molymer-containing preceramic polymer as a precursor to SiC–$MoSi_2$ ceramics, by reacting $MoCl_5$ with polymethylsilane (PMS) in tetrahydrofuran (THF) at room temperature. We also describe the processing of three-dimensionally ordered macroporous (3DOM) SiC–$MoSi_2$ composites that exhibit semiconducting behavior by embedding the developed polymer into colloidal crystal silica arrays as sacrificial templates, followed by pyrolysis at 1400 °C in an argon atmosphere and HF etching steps.

EXPERIMENTAL

Preparation of silica microspheres

The silica spheres were synthesized by a sol–gel reaction using a previously reported procedure.[22] Tetraethyl orthosilicate (TEOS, 98%, Aldrich), used as silicon source, was reacted in a mixture of anhydrous ethanol (99.9%, Aldrich), distilled water and ammonia hydroxide (25.0–28.0%, Oriental Chem. Ind.). The size range of the silica spheres was 100–700 nm, controlled by adjusting the concentration of TEOS, the reaction temperature (25–60 °C) and the concentration of ammonium hydroxide (20–130 ml). The colloidal silica prepared was then washed with ethanol (three to five times with 200 ml each) to remove impurities and then dried at 70 °C for 7–8 h.

Preparation of three-dimensionally ordered template from silica microspheres

To make close-packed silica templates, the silica microspheres (50 wt%) were redispersed in the absolute alcohol by ultrasonication for 10 min. The prepared solution was then held still for 3 h to deposit the aggregated particles that were subsequently peeled out.

The suspended spheres precipitated very slowly by natural sedimentation to form a three-dimensional ordered layer in a clean vial. After decanting the upper alcohol with a syringe, the silica deposit layer was dried at room temperature and then at 120 °C for 1 day to remove moisture on the surface.[25] All reagents were used directly without further purification.

Synthesis of PMS

Sodium was first cut in to fine particles (<2 mm) in dried THF in a glove bag filled with dry nitrogen. PMS, $[-SiH(CH_3)-]_n$, was synthesized via polycondensation of 52 ml of dichloromethylsilane (99%, Aldrich) and 23 g of cut sodium in 500 ml of THF/*n*-hexane (1 : 6) under dry nitrogen.[25] After 18 h, the synthesized polymer solution was transferred into a round-bottom flask in a vacuum through a cannula equipped with a filter tip. Oily white PMS was obtained with a yield of about 50% after evaporating the solvent. As PMS is flammable in air, it should be kept in an inert atmosphere.

Synthesis of MoPMS for SiC–$MoSi_2$ ceramic

Solutions (30 wt%) of PMS and $MoCl_5$ (99%, Aldrich) were prepared in anhydrous THF (99.9%, Aldrich) dried over sodium separately, and were mixed at room temperature to adjust the amount of $MoCl_5$ in PMS to 5 wt%, 10 wt%, 15 wt% and 25 wt%, identified hereafter as MoPMS5, MoPMS10, MoPMS15 and MoPMS25 respectively. After evaporation of the solvent, dark-brown MoPMS polymers were obtained that are no longer soluble. As PMS and $MoCl_5$ are air and moisture sensitive, all the processes were carried out under a nitrogen atmosphere.

Fabrication of macroporous SiC–$MoSi_2$

First, an as-mixed MoPMS solution containing 10 wt% $MoCl_5$ was infiltrated into the close-packed three-dimensionally ordered silica template within the pot life (48 h) of the precursor solution. The MoPMS embedded template was then vacuum dried and cured at 160 °C for 6 h to consolidate the infiltrated phase. In the pyrolysis step, the polymer–template composites were heat-treated in argon at 1 °C min^{-1} to 300 °C, held for 3 h, then heated to 1400 °C at 2 °C min^{-1} and held for 30 min. The resulting ceramic–silica composites were dipped into 20% aqueous HF for 6 h to etch out the silica template. The resulting 3DOM SiC–$MoSi_2$ ceramic was then extensively washing with distilled water until a neutral pH was attained. The samples were air dried in an oven at 110 °C overnight.

Preparation of platinum–ruthenium by borohydride reduction

In order to deposit catalysts on the inner wall of the macroporous SiC–$MoSi_2$, the resulting porous sample was dipped into a $RuCl_3$ and H_2PtCl_6 aqueous solution with a platinum/ruthenium: H_2O mole ratio of 1 : 20. After soaking for 3 h, a 1 M $NaBH_4$ solution in distilled water was added dropwise into the solution and allowed to react for 6 h. The mixture was then filtered and washed with distilled water. Then, platinum–ruthenium-supported macroporous SiC–$MoSi_2$ was finally achieved after air drying in an oven at 110 °C overnight.

Characterization

The structural changes of the polymer were analyzed with IR spectroscopy (Nicolet-360), ^{13}C and ^{29}Si solid state NMR spectroscopy (DSX600, Bruker). The morphologies of the porous samples were examined using scanning electron microscopy (SEM) (LEO1455VP) and transmission electron microscopy (TEM; EM912 Omega). Powder X-ray diffraction (XRD; Siemens D5000, Cu Kα) was performed to determine the crystalline phases and structures of the ceramics. Thermogravimetric analysis (TGA; TA Instrument 2950) was performed at 10 °C min^{-1} to 1000 °C in air. BET surface areas were determined by nitrogen adsorption–desorption isotherms (ASAP 2400, Micromeritics).

RESULTS AND DISCUSSION

It is well known that PMS produced by sodium dehalocoupling of $MeHSiCl_2$ is a soluble preceramic polymer with a low molecular weight ($M_w = 1218$, $M_n = 578$) and a low ceramic yield of 43%; furthermore, on heating, it converts to SiC with excess silicon. As the PMS is mixed with $MoCl_5$ in THF at room temperature, HCl is released in an exothermic reaction. In addition, the liquid mixture gradually turns to a dark gel after 30–100 h and finally becomes a fragile solid after 1 week even at room temperature. It is generally observed that the gel time becomes shorter with increasing amounts of $MoCl_5$ and the use of hydrophilic solvents. As summarized in Table 1, the insoluble products obtained show significantly improved ceramic yields, possibly due to enhanced curing of the precursor by $MoCl_5$. MoPMS10 prepared with 10% $MoCl_5$ showed the highest ceramic yield (about 88%), whereas MoPMS with >10% MoCls evolved $SiCl_x$ or $MoCl_5$ by evaporation at higher temperature, resulting in decreased ceramic yields. Thus, it became important to investigate the curing reaction chemistry of these mixtures.

From IR spectroscopy (shown in Fig. 1), one can observe ν(Si–H) peaks at 2100 and 930 cm^{-1} and ν(Si–C) at 1250 cm^{-1} in PMS decrease with increasing amounts of $MoCl_5$. In addition to the self-curing of PMS (Eqns (1) and (2)), it is most likely that reactions between Si–H or Si–CH_3 and Mo–Cl bonds are involved with HCl elimination to form Si–Mo (Eqn (3)), which promoted the curing degree of PMS and resulted in insoluble products.

$$\equiv Si{-}H + H{-}Si\equiv + MoCl_5 \longrightarrow \equiv Si{-}Si\equiv + MoCl_3 + 2HCl\,(g) \quad (1)$$

$$\equiv Si{-}H + \equiv Si{-}CH_3 + MoCl_5 \longrightarrow \equiv Si{-}CH_2{-}Si\equiv + MoCl_3 + 2HCl\,(g) \quad (2)$$

$$\equiv Si{-}H + MoCl_5 \longrightarrow \equiv Si{-}MoCl_4 + HCl\,(g) \quad (3)$$

In the ^{29}Si NMR spectrum shown in Fig. 2a, PMS displays a broad peak at around −70 ppm, which corresponds to the overlap of Si–(Me*Si*H)–Si (−45 to −55 ppm) and Si–(Me*Si*)=Si_2 (−60 to −75 ppm) in the polymer chain, and the small peak at −35 ppm is assigned to the terminal Si–(Me*Si*H)H and Si–(Me*Si*H)Cl.[28]

When PMS reacts with $MoCl_5$, the two signals observed at around −70 ppm and −35 ppm are broadened, which likely originate from increases in the numbers of Si–(Me*Si*)=Si_2 (shown in Eqn (1)) and the two kinds of terminal groups respectively. In addition, two smaller peaks at 0 to −20 ppm appear. There are two possible assignments: (1) one is very likely to be *Si*–Mo (shown in Eqn (3)), although this needs to be proved further; (2) or the other could be Si_2–*Si*–C_2 units formed from the further crosslinked products shown in Eqn (2). In the case of the ^{13}C NMR spectra shown in

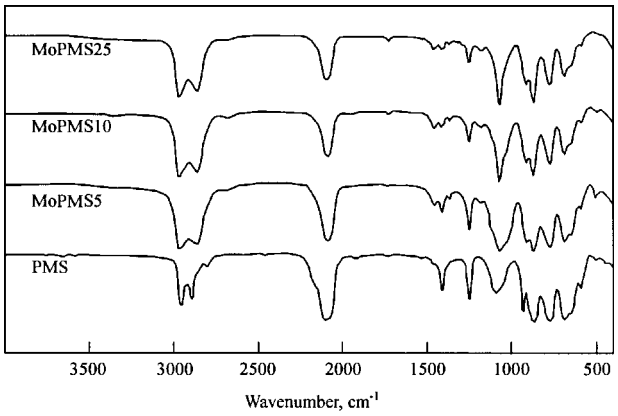

Figure 1. IR spectra of the various polymeric precursors.

Table 1. The gel time at room temperature in nitrogen and ceramic yield at 1400 °C in argon of the cured insoluble polymeric MoPMS precursors

	PMS	MoPMS5	MoPMS10	MoPMS15	MoPMS25
Mo/Si (atom ratio)	0	0.008	0.018	0.028	0.054
Gel time[a] (h)	>10 000	100	48	40	30
Ceramic yield[b] (%)	43.0	78.1	87.0	68.7	57.4

[a] Time to become the gel phase right after mixing.
[b] Ceramic residue when pyrolyzed up to 1400 °C.

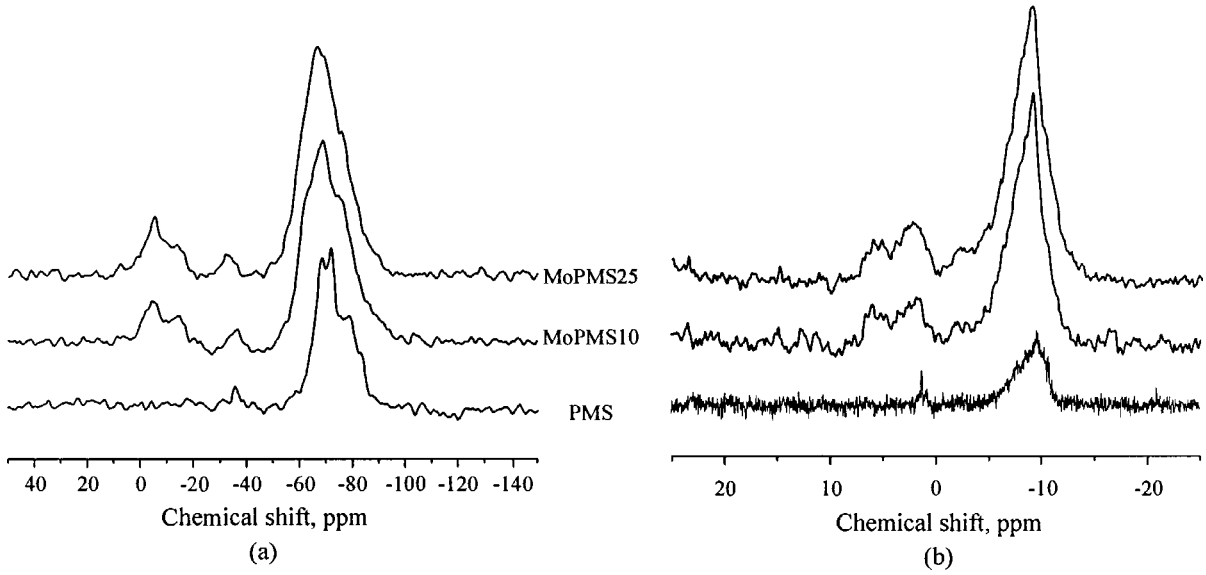

Figure 2. (a) ^{29}Si NMR and (b) ^{13}C NMR spectra of the polymers obtained (solid NMR was performed on MoPMS25 and MoPMS10; liquid NMR was performed on the PMS sample).

Fig. 2b, the signal around −10 ppm is assigned to Si–CH_3;[29] however, small and broadened signals at 2 and 8 ppm appeared for the MoPMS products, which may be assigned as CH_3–Si–Mo or Si–CH_2–Si, although these assignments need further proof. In addition, the reactivity of Si–H with metal chlorides was also reported by Kriventsov's group, who successfully synthesized titanium- and zirconium-containing polycarbosilane (PCS) from reactions of Si–H bonds in PCS with $TiCl_4$ and $ZrCl_4$ respectively.[15,16] From the above analysis, it is clear that $MoCl_5$ could also further dehydrocoupled addition to crosslinking of PMS and hence increase the ceramic yield.

Figure 3 shows powder XRD patterns of the pyrolyzed (1400 °C) samples of PMS and MoPMS10. The PMS-derived ceramic sample displays four peaks at 28.5°, 36°, 61° and 72° (Fig. 4a), which are assigned to free silicon, β-SiC (111), β-SiC (220) and β-SiC (311) respectively.[30] In the diffraction pattern of MoPMS10 (Fig. 4b), some Mo–Si phases appear accompanied with the SiC matrix with no free silicon. It is reasonable to assume that the excess silicon reacts with molybdenum to form $MoSi_2$ with a minor Mo_5Si_3 phase at high temperature.[21] In addition, it should be noted that MoPMS10-derived SiC–$MoSi_2$ ceramic exhibits a higher degree of crystallinity than that of PMS-derived SiC ceramic, which implies that introduction of molybdenum contributes to the crystallization of the porous SiC matrix.

The solution of preceramic polymer MoPMS10, which gives the highest ceramic yield after drying, curing and pyrolysis (Table 1), was used to infiltrate and fill the void spaces within the template consisting of a three-dimensionally ordered crystalline array of silica spheres within the pot life (48 h). After pyrolysis at 1400 °C and subsequent removal of the silica template, sphere-inversed 3DOM ceramic structures

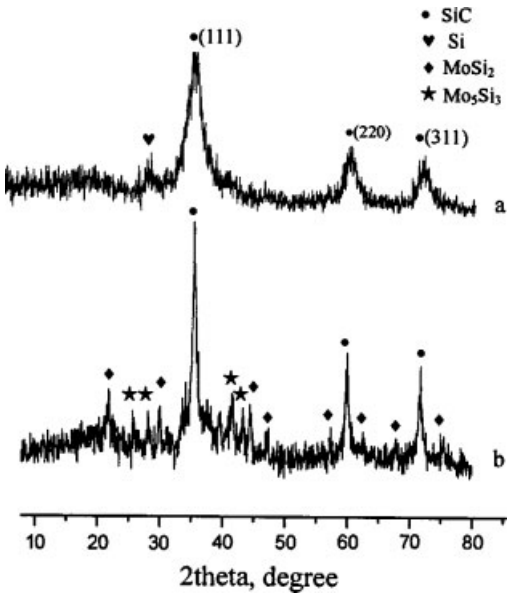

Figure 3. Powder XRD patterns of (a) PMS-derived and (b) MOPMS10-derived ceramics, pyrolyzed at 1400 °C in argon.

were produced. Fig. 4a–c) shows three representative SEM images of various pore-size samples with flat plane or deep-seated structures. It is generally observed that highly ordered and interconnected 'honeycomb' pore structures are obtained by replicating the long-range and three-dimensionally close-packed silica template.

The 3DOM structures of the resulting porous ceramics with different pore sizes were further characterized by TEM and are shown in Fig. 5. In each image in Fig. 5

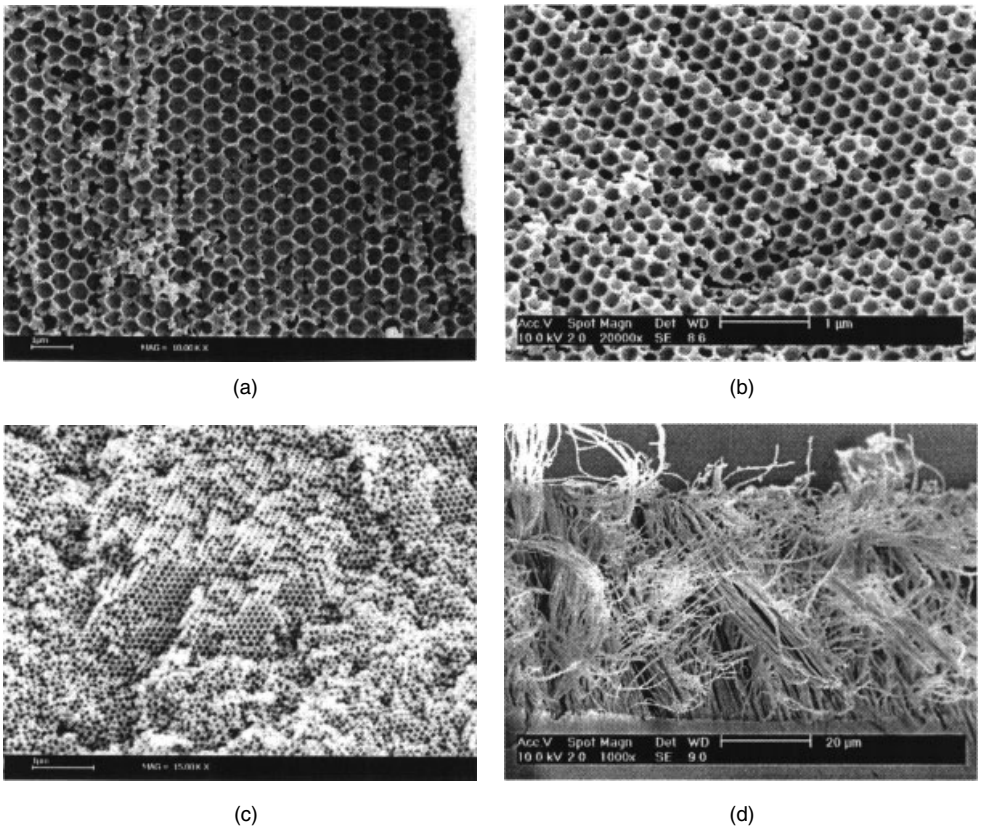

Figure 4. SEM images of 3DOM SiC–$MoSi_2$ ceramic with pore sizes of about (a) 475 nm, (b) 210 nm, (c) 93 nm. (d) SiC–$MoSi_2$ nanofiber from 200 nm alumina membrane.

the dark areas represent the ceramic frameworks and the light areas are void space. It is clear that the resulting porous ceramics exhibit regular three-dimensionally ordered structures. Different views of the pore array can be classified as corresponding to the different planes of an h.c.p. structure, such as (211) (Fig. 5a), (111) (Fig. 5b and d) and (110) (Fig. 5c).[25] The small openings of about 70 ± 10 nm connecting the macropores further illustrate the long-range, three-dimensional order of the ceramic structures. In addition, when MoPMS10 was embedded into an alumina membrane template with 100–200 nm cylindrical pores, after conversion to ceramic and template removal, the result was a rod-like morphology, as shown in Fig. 4d.

The pore characteristics of the macroporous SiC–$MoSi_2$ ceramic obtained were investigated using the nitrogen adsorption method and the results are summarized in Table 2. The pore sizes of about 90 to 475 nm were approximately proportional to the sizes 105 to 500 nm of the sacrificial silica sphere templates with 5–10% shrinkage, which is quite different from the 25–30% shrinkage of the pure PMS-derived porous samples obtained by the identical process.[25] This can be attributed to the molybdenum promoted crosslinking of the precursor, leading to a higher ceramic yield.

It was observed that the BET surface areas and the pore volumes of the porous samples increased as the diameters of the silica spheres decreased, while the pore sizes showed the opposite trend. This can be interpreted as the smaller silica spheres producing higher contact areas per unit volume between the silica and the infiltrated polymeric precursor, which develop a higher surface area. In particular, when 105 nm silica spheres are used as the template, the related porous ceramic has a considerably higher surface area and pore volume of about 407.6 $m^2\ g^{-1}$ and 0.46 $cm^3\ g^{-1}$ respectively than those of previously prepared oxide ceramics, where average surface areas of about several 10–150 $m^2\ g^{-1}$ are reported,[26,27,31] although they are smaller than those of mesoporous carbon materials (>1000 $m^2\ g^{-1}$).[32]

Figure 6 shows a representative adsorption and desorption isotherm plot and the pore-size distribution of a 475 nm porous SiC–$MoSi_2$ sample. The isotherm curve displays typical type II nitrogen adsorption behavior with the hysteresis loop at medium pressure, which indicates the existence of cylindrically shaped pores.[25] From the pore-size distribution curve (Fig. 6 inset), the broad peak at 60–80 nm and the sharp peak at 3–5 nm prove the existence of macropores and near-micropores respectively. The former originate from the contacting points between initial neighboring silica spheres. However, it is believed that the near-micropores were formed by etching out silica

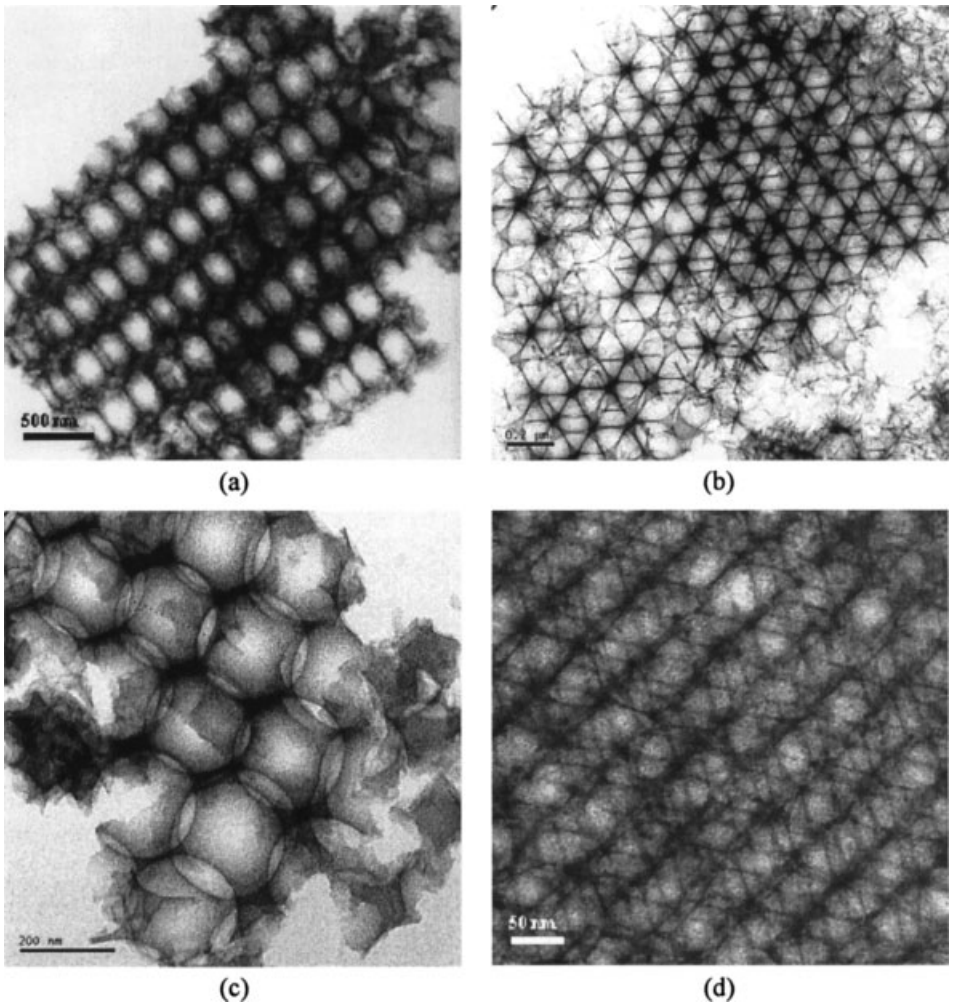

Figure 5. TEM images of 3DOM SiC–$MoSi_2$ with different pore sizes: (a) 475 nm, (211); (b) 210 nm, (111); (c) 210 nm, (110); (d) 93 nm, (111).

Table 2. Pore characteristics of the macroporous SiC–$MoSi_2$ ceramic

SiO_2 sphere (nm)	Macropore size of the ceramic (nm)	BET surface area ($m^2\ g^{-1}$)	Pore volume ($cm^3\ g^{-1}$)
105	93	407.6	0.46
228	210	321.2	0.28
500	475	232.4	0.12

diffused into the ceramic framework from the silica template during high-temperature pyrolysis. In addition, smaller particles with higher surface activity might cause more significant diffusion to develop pores in the walls of the ceramic frameworks, resulting in a higher surface area. Similar diffusion phenomena at the interface were reported for spin-coated BN films on SiO_2-modified silicon wafers, where oxygen from the silica layer diffused into the BN layer at 1100 °C.[33,34] Thus, it can be concluded that the porous

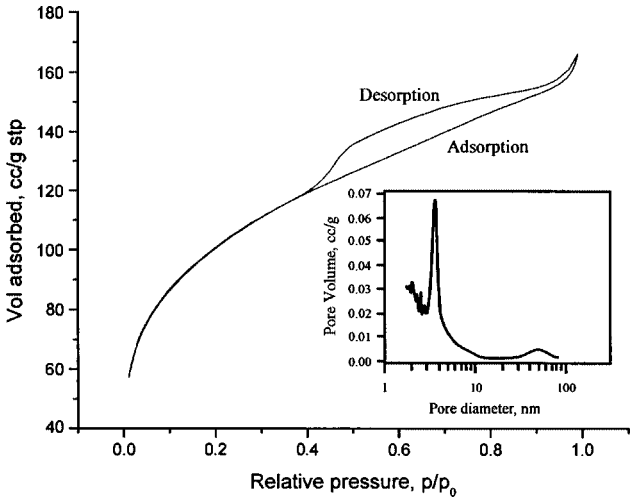

Figure 6. Nitrogen adsorption and desorption isotherms of the 475 nm porous SiC–$MoSi_2$ ceramic. Inset: the corresponding pore-size distribution curve calculated from the adsorption branch of the nitrogen isotherm by the BJH method.

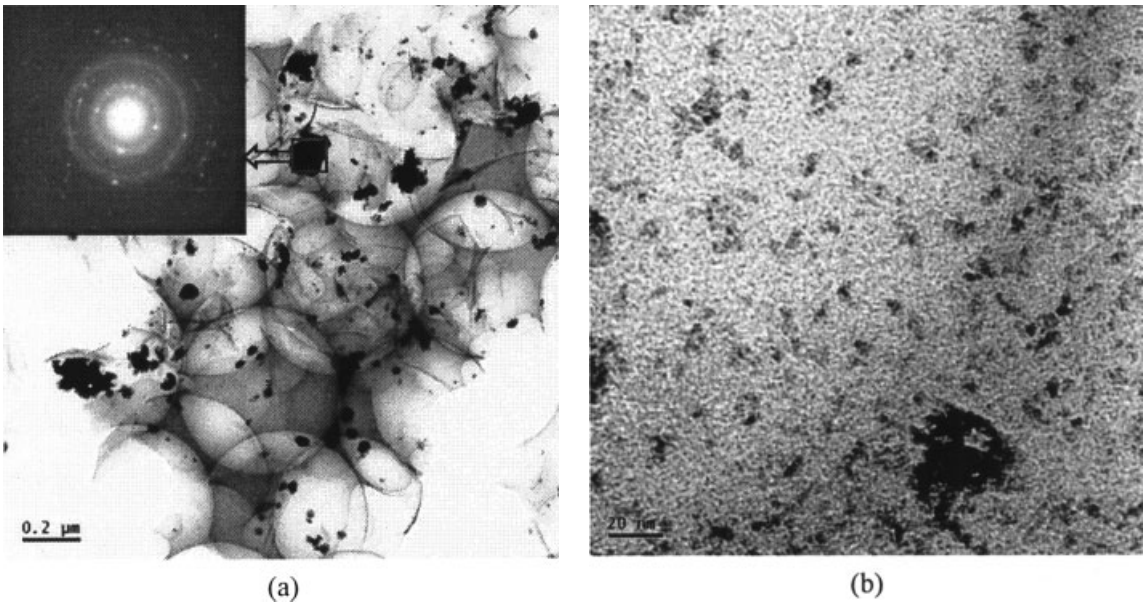

Figure 7. (a) TEM image and (b) high-resolution TEM image of the 475 nm porous SiC–$MoSi_2$ ceramic with platinum–ruthenium supported on the walls of the surface. Inset: electron diffraction of the particle aggregate.

ceramic obtained exhibits a trimodal pore-size distribution, originating from the template spheres, contact points between the spheres and partially diffused silica.

For fuel cells and other catalytic applications, metallic nanoparticles are usually supported on a high-surface-area substrate so that they can work either as an electrode material or as a catalyst. Here, the porous SiC–$MoSi_2$ ceramic obtained was surface-treated with platinum–ruthenium nanoparticles produced by borohydride reduction under mild chemical conditions.[35] TEM images (Fig. 7a) show that the porous framework with a 475 nm pore size was coated with randomly aggregated platinum–ruthenium nanoparticles on the surface of the wall. Moreover, high-resolution TEM (Fig. 7b) reveals that the 10 nm platinum–ruthenium particles or the aggregates are homogeneously deposited on the surface. Electron diffraction (Fig. 7a inset) of the particles proves the existence of (111), (200), (220) and (311) platinum–ruthenium, which is consistent with a solid-solution phase as reported previously.[36]

In addition, using a modified two-point method, the electrical properties of the MoPMS-derived SiC–$MoSi_2$ ceramic were analyzed for the rod-like structure loaded in the alumina membrane template with 200 nm pores (shown in Fig. 8, inset). It can be seen that the specific resistance of the 200 nm SiC–$MoSi_2$ nanorods has a negative temperature dependence, changing from about 8.3 Ωm to 4.2×10^{-2} Ωm in going from 20 to 300 K, i.e. shows semiconductor-like behavior (Fig. 8). This is relatively lower than that of PCS-derived SiC fibers (Nicalon fiber, NL-200), with specific resistances of about 10^1–10^2 Ωm.[37] It is believed that the electrically conductive $MoSi_2$ phase[38] in the SiC–$MoSi_2$ ceramic contributes to the higher conductivity of the

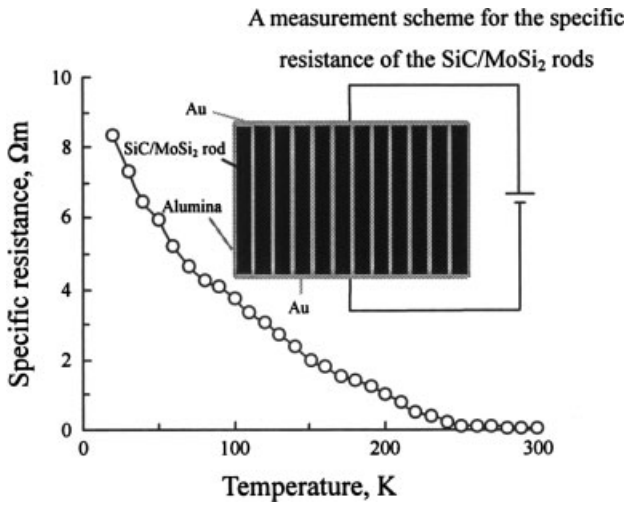

Figure 8. Temperature dependence of the specific resistance of 200 nm SiC–$MoSi_2$ rods. Inset is a measurement scheme for the specific resistance of the SiC–$MoSi_2$ rods.

composite phase. Based on the electrical properties of the SiC–$MoSi_2$ ceramic, it may be possible to develop a low-resistance heating nanodevice and a new IR sensor for a human body detector using SiC–$MoSi_2$ as an element of the sensor.[37,38]

Finally, the SiC–$MoSi_2$ porous composite showed excellent thermal stability, compared with PMS-derived porous SiC samples. When exposed to air up to 1000 °C, the former sample showed almost no weight change, whereas the latter displayed an 8 wt% gain due to oxidation of the excess silicon

starting from 500 °C, as is well documented.[25,30] Therefore, the porous SiC–$MoSi_2$ ceramic with semiconductor behavior appears to be a promising material for high-temperature applications of electrically heated filters and membranes.

CONCLUSIONS

The sacrificial template method used to synthesize well-ordered nanostructures, especially those constituting replicas of the templates, is remarkably useful for microfabrication applications. In this study, a high-temperature stable porous SiC–$MoSi_2$ ceramic, with a specific resistance ranging from about 8.3 to 4.2×10^{-2} Ωm over the range 20 to 300 K, was successfully fabricated with an $MoSi_2$ phase embedded in the SiC matrix, using $MoCl_5$-modified PMS as the preceramic polymer by combining with silica array templates. Macroporous SiC–$MoSi_2$ with three-dimensionally long-range-ordered structures exhibit high surface areas and pore volumes ranging from 407.6 to 232.4 $m^2\ g^{-1}$ and 0.46 to 0.12 $cm^3\ g^{-1}$ respectively, which can be easily tailored by using different sizes of template spheres. In addition, the macroporous SiC–$MoSi_2$ can be used as a catalyst support, as suggested by the successful deposition of platinum–ruthenium in the pores.

Acknowledgements

We acknowledge Korea Science and Engineering Foundation (KoSEF), grant no. 2000-2-30700-007-3 and the Chinese Natural Science Fund, grant no. 59972042, for financial support. We also give thanks to the Korea Basic Science Institute for SEM support.

REFERENCES

1. Segal D. *Chemical Synthesis of Advanced Ceramic Materials*. Cambridge University Press: New York, 1991.
2. Birot M, Dunogues J. *Chem. Rev.* 1995; **95**: 1443.
3. Bill J, Aldinger F. *Adv. Mater.* 1995; **7**: 775.
4. Liu Q, Wu HJ, Lewis R, Maciel GE, Interrante LV. *Chem. Mater.* 1999; **11**: 2038.
5. Verbeek W, Winter G. *German Patent* 2 236 078, 1974.
6. Yajima S, Okamura K, Hayashi J, Omori M. *J. Am. Ceram. Soc.* 1976; **59**: 324.
7. Ginzburg M, Maclachlan MJ, Yang SM, Coombs N, Coyle TW, Raju NP, Greedan JE, Herber RH, Ozin GA, Manners I. *J. Am. Chem. Soc.* 2002; **124**: 2625.
8. Vaahs T, Brück M, Wöcker WDG. *Adv. Mater.* 1992; **4**: 224.
9. Mucalo MR, Milestone NB, Vickridge IG, Swain MV. *J. Mater. Sci.* 1994; **29**: 4487.
10. Lücke J, Keuthen M, Ziegler G. In *Proceedings of the Fourth Euro-Ceramics*, vol. 4. Faenza Editrice: Italy, 1995; 187.
11. Ziegler G, Kleebe HJ, Motz G, Müller H, Traßl S, Weibelzahl W. *Mater. Chem. Phys.* 1999; **2506**: 1.
12. Galloro J, Ginzburg M, Miguez H, Yang SM, Coombs N, Safa-Sefat A, Greedan JE, Manners I, Ozin GA. *Adv. Funct. Mater.* 2002; **12**: 382.
13. Ishikawa T, Kohtoku Y, Kumagawa K, Yamamura T, Nagasawa T. *Nature* 1998; **391**: 773.
14. Yajima S, Iwai T, Yamamura T, Okamura K, Hasegawa Y. *J. Mater. Sci.* 1981; **16**: 1349.
15. Gubin SP, Moroz EM, Boranin AI, Kriventsov VV, Zyuzin DA, Popova NA, Florina EK, Tsirlin AM. *Mendeleev Commun.* 1999; **2**: 59.
16. Kriventsov VV, Zyuzin DA, Bogdanov SV, Moroz EM, Gubin SP, Tsirlin AM, Popova NA. *Nucl. Instrum. Methods Phys. Res. A* 2000; **448**: 314.
17. Lichtenberger O, Pippel E, Woltersdorf J, Riedel R. *Mater. Chem. Phys.* 2003; **81**: 195.
18. Matthew JA, Carolyn EJ, David AR. *J. Organometal Chem.* 1993; **443**: 137.
19. Petrovic JJ, Vasudevan AK. *Mater. Sci. Eng. A* 1999; **261**: 1.
20. Yamada K, Kamiya N. *Mater. Sci. Eng. A* 1999; **261**: 270.
21. Kim DP. *Mater. Res. Bull.* 2001; **36**: 2497.
22. Yu JS, Yoon SB, Chai GS. *Carbon* 2001; **39**: 1421.
23. Bartlett PN, Birkin PR, Ghanem MA, Toh CS. *J. Mater. Chem.* 2001; **11**: 849.
24. Yi DK, Kim DY. *Nanolett.* 2003; **3**: 207.
25. Wang H, Li XD, Yu JS, Kim DP. *J. Mater. Chem.* 2004; **14**: 1383.
26. Stein A, Schroden RC. *Curr. Opin. Solid State Mater. Sci.* 2001; **5**: 553.
27. Yan H, Blanford CF, Holland BT, Smyrl WH, Stein A. *Chem. Mater.* 2000; **12**: 1134.
28. Narisawa M, Yoshida T, Iseki T, Katase Y, Okamura K. *Chem. Mater.* 2000; **12**: 2686.
29. Boury B, Bryson N, Soula B. *Appl. Organometal. Chem.* 1999; **13**: 419.
30. Cao F, Kim DP, Li XD. *J. Mater. Chem.* 2002; **12**: 1213.
31. Holland BT, Blanford CF, Do T, Stein A. *Chem. Mater.* 1999; **11**: 795.
32. Jun S, Joo SH, Ryoo R, Kruk M, Jaroniec M, Liu Z, Ohsuna T, Terasaki O. *J. Am. Chem. Soc.* 2002; **122**: 10 712–.
33. Kho JG, Moon KT, Nouet G, Ruterana P, Kim DP. *Thin Solid Films* 2001; **389**: 78.
34. Kho JG, Moon KT, Kim JH, Kim DP. *J. Am. Ceram. Soc.* 2000; **83**: 2681.
35. Jung DH, Hong SH, Peck DH, Shin DR, Kim ES. *Carbon Sci.* 2003; **4**: 121.
36. Zhang X, Chan KY. *Chem. Mater.* 2003; **15**: 451.
37. Ishikawa T. *Compos. Sci. Technol.* 1994; **51**: 135.
38. Cordelair J, Greil P. *J. Am. Ceram. Soc.* 2001; **84**: 2256.